A Multisource Energy Harvesting Utilizing Highly Efficient Piezoelectric PMN-PT Single Crystal

Almuatasim Alomari[1], Ashok Batra[1], Mohan Aggarwal[1] and C. R. Bowen[2]

[1]Department of Physics, Chemistry, and Mathematics
(Materials Science Group-Clean Energy Laoratory)
College of Engineering, Technology and Physical Sciences
Alabama A&M University
Normal, AL 35762 USA.
[2]Department of Mechanical Engineering, University of Bath, Bath UK

Abstract

A multi-source Energy Harvester employing simultaneously piezoelectric and pyroelectric effects in lead magnesium niobate-lead titanate (PMN-PT) single crystal is demonstrated. The article presents a study of PMN-PT with (67:33) composition single crystal grown in our laboratory via a vertical gradient freeze method with no flux. The performances of the piezoelectric and pyroelectric energy harvester using unimorphs were evaluated via modeling and experiments. The theoretical study was implemented based on single degree-of-freedom model. The modelling procedure was approximated using finite element method to predict the electromechanical behavior of these harvesters. The maximum power density at resonance frequency 51 Hz and optimum resistance of 7 kΩ was 5.2 μW/ (g^2 cm^3) under acceleration of vibration base of 1 g. The measured values of electrical output parameters were in good agreement with theoretical and modelling results using MATLAB and COMSOL Multiphysics respectively. By using pyroelectric effect along with the piezoelectric one, the output voltage of energy harvester was found to be enhanced at optimum resistance and different frequency values. It has been noticed that the output voltage is increased monotonically with temperature-difference (ΔT).

KEYWORDS: energy harvesting, pyroelectric, and piezoelectric effects, PMN-PT

1. Introduction

Energy harvesting (power harvesting or energy scavenging) is the process by which electrical energy is derived from ambient sources such as solar, thermal, wind and kinetic energy, captured, and stored for powering ultra-small, wireless autonomous devices. Piezoelectric energy harvesting from mechanical external vibrations has received significant attention in the past decade. However, pyroelectric energy harvesting, in which time-dependent temperature fluctuations are converted into electrical energy via pyroelectric effect, is not widely explored (Bowen et al., 2014). To enhance or supplement the performance of the energy harvesting device, it is fascinating and useful to develop a technology to simultaneously or individually harvest both the mechanical and thermal energies via an integrated device. Fortunately, there are smart materials, so called ferroelectrics (such as, lead zirconate titanate-PZT, lead magnesium niobate-lead titanate-PMN-PT) which have desired both the piezoelectric and pyroelectric properties.

Recently, Piezoelectric energy harvesting in $Pb(Mg_{1/3}Nb_{2/3})O_3$-$PbTiO_3$ (PMN-PT) single crystal has been successful in producing sufficient power for medical devices and micro-wireless sensor applications (Roundy & Wright., 2004, Hong et al., 2004, Radziemski & Lynn., 2004, Green, Mossi, & Bryant 2005, Badel et al., 2006, Ren et al., 2006, Song et al., 2009, Kim et al., 2010, Leadbetter, Brown, & Adamson., 2013, Hwang et al., 2014, Kazys, Sliteris, & Sestoke, 2015). It has been possible due to the fact that the piezoelectric strain and electromechanical coupling coefficients of PMN-PT is higher than other piezoceramics such as PZT. It is also a nondestructive material with high toughness, high dielectric constant and low dielectric loss (Choi et al., 1989, Bai et al., 2000., Zawilski et al., 2003., Uchino, 2009). Vibration energy harvester (VEH) devices using PMN-PT single crystal has been examined due to their simple structure, high power density, and accurate response under mechanical stimulus (Seung et al., 2011, Tang et al., 2014).

Several experiments and analytical models on the PMN-PT single crystal have been implemented in order to measure and improve energy harvesting performance. For instance, Sun et al., developed a new model to predict the output power of PMN-PT single crystal attached at the clamped end of aluminum beam in static and dynamic case using constitutive equations and single degree of freedom (SDOF) model. The maximum value of the output power was about 0.586mW at the resistive load of 94.7 kΩ, with a good match between the measured and the calculated results (Sun et al., 2008). Song et al., investigated the performance of a vibration energy harvester (VEH) employing a single crystal lead magnesium niobate-lead titanate (PMN-PT) material via analysis and experiment. The maximum dc power generated was 19 mW for an excitation of 0.2 g (song et al., 2009). Ren et al. measured and analyzed the output voltage and power of a PMN-PT single crystal beam with tip mass. Their results showed that the maximum voltage and power are 91.23 V and 4.16 mW, respectively at resonance frequency of 60 Hz and tip mass about 0.5 g under a cyclic force of 0.05 N (Ren et al., 2010). In 2011 Moon et al., fabricated and analyzed a piezoelectric energy harvesting device using a Zr-doped PMN-PT

piezoelectric single-crystal beam. The device generated a power of 0.3 mW with an optimal resistive load of about 50 kΩ from 0.1 g acceleration at its resonant frequency of 57 Hz, which was similar to the calculated results (Moon et al., 2011). In 2012 a new model of piezoelectric cantilever with $0.71Pb(Mg_{1/3}Nb_{2/3})O_3–0.29PbTiO_3$ single crystal and brass shim has been studied using constitutive equations of d_{15} mode and single degree of freedom. The maximum value obtained of output power at resonance frequency 65 Hz was 8 mW at load resistance of 1 MΩ and acceleration amplitude of vibration base of 10 m/s^2 with good agreement between the measured and proposed modeling results (Zhou et al., 2012). In recent years, Hwang et al. reported an elastic PMN-PT single crystal energy harvester for a self-powered cardiac pacemaker. The authors claimed that the energy-harvesting device generates a short-circuit current of 0.223 mA and an open-circuit voltage of 8.2 V (Hwang et al., 2014).

In the present work, with the aim of simultaneously harvest thermal and mechanical energies, a single crystal of PMN-PT with (67:33) composition was grown in our laboratory via a vertical gradient freeze method with no flux. The performance of piezoelectric and pyroelectric energy harvesting device based on PMN-PT single crystal were evaluated and demonstrated via modeling and experiments. Thus, proving the concept of improving the performance of Energy Harvester via a multifunctional materials system.

2. Experiment Procedure

2.1 Synthesis and Crystal Growth

Single crystals of lead magnesium niobate-lead titanate (PMN-PT) with the chemical structural formula $Pb(Mg_{1/3}Nb_{2/3})O_3$-$PbTiO_3$ in the ratio 67:33 were synthesized using stoichiometric amounts of the high purity materials: PbO, MgO, Nb_2O_5 and TiO_2. Raw powders were weighed with desired molar ratios. The initial weights for a charge of one mole of PMN-PT solid solutions (volume density equals 8.2 g/cm^3) were calculated to be consisted of 8.96 g of MgO, 59.10 g of Nb_2O_5, 26.63 g of TiO_2, and 223.19 g of PbO. The dry powders were mixed for a desired period of time using a tumbling mill.

The vertical gradient freeze method with no flux was used to obtain PMN-PT single crystals. The system PMN-PT (67/33) was loaded in a platinum crucible covered with an alumina lid. Due to high volatility of PbO, the crucible was sealed by means of alumina cement. The crystal growth was carried out in a cylindrical furnace equipped with a programmable temperature controller. An optimized thermal profile was used for the growth of PMN-PT crystals by spontaneous nucleation, namely: (i) heating from room temperature to 900°C at a ramp rate of 150°C/h and dwelling for 6 h; (ii) heating at 100°C/h to 1305°C and dwelling for 24

h; (iii) slow cooling from 1305°C to 1100°C at 2°C/h, from 1100°C to 1000°C at 3°C/h, from 1000°C to 800°C at 5°C/h, then from 800°C down to room temperature at 20°C/h. This slow cooling process was applied to obtain a more stable growth. In order to get bigger sized PMN-PT single crystals, the growth process was repeated for three times. In each time, a lead loss of about 1 wt% was observed by checking the weight difference before and after growth run. To overcome this problem, 1 wt% of excess PbO was added to the charge to compensate the lead loss.

2.1 Dielectric and Pyroelectric Coefficient Measurements

Both the real and imaginary parts of the dielectric constant (ε', ε'') for a poled sample of an PMN-PT single crystal with dimensions of 8×5×1.62 mm^3 at different frequencies were measured as a function of temperature. The sample was heated to around 215ºC and the temperature dependence of the dielectric data (capacitance and tanδ) was measured at a rate of 3°C/min. Values of dielectric constant (ε') and dielectric loss (ε'') were then calculated for each value of the capacitance.

The temperature dependence of the pyroelectric coefficient for a poled sample of an PMN-PT single crystal have been studied. Silver electrodes were printed on both sides of the sample and it then was poled with an appropriate electric field. The pyroelectric current was measured using a 6517B Keithley electrometer and temperature was measured by an HP34970 digital multimeter. The pyroelectric coefficient p was calculated via the following equation:

$$p = \frac{I/A}{dT/dt}$$

where I is the pyroelectric current, A is the area of electrodes and (dT/dt) is the rate of change of temperature. The measurements were automated using LabVIEW 6i software and all the raw data were collected by PC and stored in a file. The variation of ac conductivity for the PMN-PT single crystals as a function of temperature has also been studied at a frequency of 1 kHz. It can be presented in term of the dielectric loss ε'' by the following relation:

$$\sigma = \omega \varepsilon_o \varepsilon''$$

where ω is the angular frequency = 2πf. For this frequency, the conduction was described by a thermally activated process with the relation:

$$\sigma = \sigma_o \exp(-E_{ac} / k_B T)$$

where σ_o is a constant, k_B is the Boltzmann's constant, and E_{ac} is the activation energy for conduction.

3.0 Analysis and modelling of vibration energy harvester (VEH)

3.1 Design and testing VEH

The design of VEH device investigated was a unimorph beam with a clamped-free end. A PMN-PT single crystal ws sandwiched between two conducting silver electrodes and positioned on the top of clamped-end of aluminum beam. A proof mass is attached at the free end as shown in Figure 1. The experimental set-up consists a mini mechanical shaker, function generator to produce different frequencies, high-power amplifier to produce a cyclic force of required magnitude and frequency, accelerometer sensors to measure the acceleration of vibration base via picoscope, multimeter to measure the output voltage from the harvester, picoscope interfaced to computer, laser displacement meter to measure the displacement of the cantilever beam, variable impedance module, breadboard, capacitor, rechargeable battery, and AC-DC circuit. To avoid any interference from the noise in the surrounding environment, all experiments were performed on an isolated optical bench. The PMN-PT single crystal is glued on a flex cantilever substrate that is mounted on a shaker. The shaker is excited by an amplifier module to generate vibrations. Under exciting vibration, the piezoelectric harvester produces AC electrical output. Then, the output signal from the harvester is connected to a variable resistive load or an AC-DC circuit with a capacitive load. The mechanical and piezoelectric properties of the unimorph cantilever beam are summarized in Table 1.

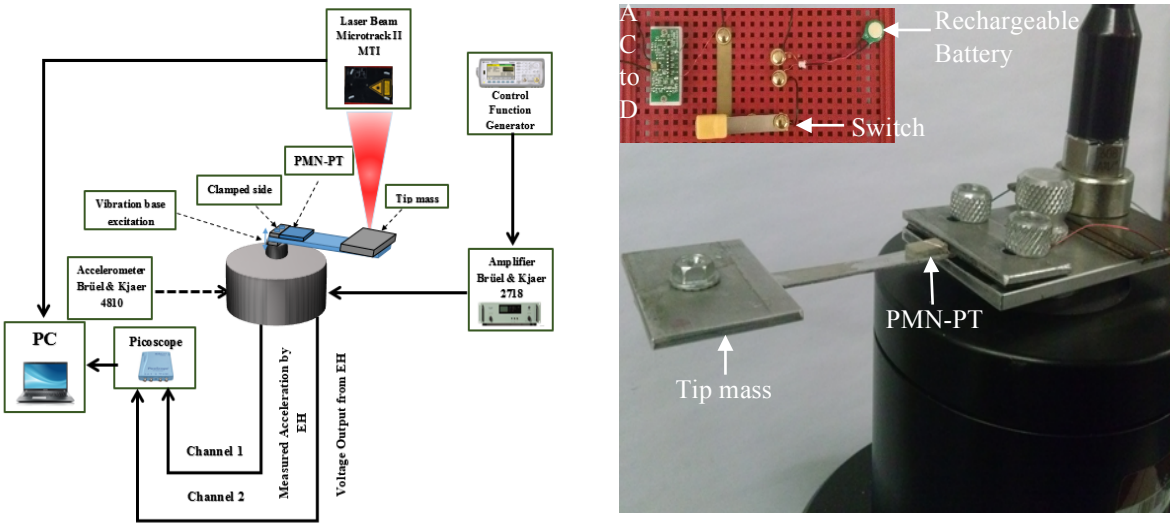

(a) (b)

Figure 1. (a) Experimental setup used for piezoelectric energy harvesting measurements of a unimorph cantilever beam (b) Magnified view of VEH tested under base excitation

Table 1. The mechanical and piezoelectric properties of unimorph cantilever beam

Parameters	Properties
Beam length/width/thickness	60/5/1 mm
PMN-PT single crystal length/width/thickness	8/5.1/1.62 mm
Density of substrate material (ρ_s)	2700 kg/m^3
Density of piezoelectric material (ρ_p)	8100 kg/m^3
Substrate Young's modulus (E_s)	70 GPa
Piezoelectric Young's modulus (E_p)	72 GPa
Dielectric constant (ε)	53.1×10^{-9} F/m
Piezoelectric coefficient (d_{31})	850×10^{-12} N/C
Coupling factor (k_{31})	0.21
Damping ratio coefficient of Al beam (ζ)	0.034
Damping coefficient (C)	0.138
Mass of tip mass with	6.03 g

3.1 Analysis procedure

Under influence of a periodical force on the clamped-end of the beam in the vertical direction, the maximum electrical output of PMN-PT film can be harvested at resonance frequency of the beam. The steady-state solution of output voltage can be obtained as (Erturk and Inman., 2008):

$$v(t) = \frac{\sum_{r=1}^{\infty} \frac{j\omega F_r \chi_r}{\omega_r^2 - \omega^2 + j2\xi_r \omega_r \omega}}{\sum_{r=1}^{\infty} \frac{j\omega \chi_r^2}{\omega_r^2 - \omega^2 + j2\xi_r \omega_r \omega} + \frac{1}{R_l} + j\omega C_p} e^{i\omega t}$$

where v is the generated voltage over the thickness of the piezoelectric layer; ζ_r is the damping ratio, ω_r is angular resonance frequency; χ_r is the modal electromechanical coupling term; F_r is the modal mechanical forcing term; C_p is the piezoelectric capacitance and R_l is the resistive load.

The average power output can be obtained as:

$P=v(t)^2/2R_l$

The resonance frequency of the unimorph cantilever beam with tip mass is given as:

$$f_r = \frac{1}{2\pi}\sqrt{\frac{3EI}{mL^3}}$$

where EI, m are the flexural rigidity and equivalent mass, respectively and are given by:

$$m = 0.236m_b + m_t$$

$$EI = \frac{w}{12}\left[E_s t_s^3 + E_s(t_b^3 - t_a^3) + 4E_p(t_c^3 - t_b^3)\right]$$

$$t_c = \frac{(t_p^2 + 2nt_p t_s + nt_s^2)}{2(t_p + nt_s)},\ t_b = t_c - t_p,\ t_a = \frac{(t_p^2 + 2t_p t_s + nt_s^2)}{2(t_p + nt_s)},\ n = \frac{E_p}{E_s}$$

E_s: is the Young's modulus of substrate material
E_p: is the Young's modulus of piezoelectric material
t_s: is the thickness of substrate material
t_p: is the thickness of piezoelectric material
w: is the width of substrate/ piezoelectric material
L: is the length of aluminum beam
m_b: is the mass of aluminum beam
m_t: is the mass of tip mass

The piezoelectric voltage constant (g_{33}) and Young's modulus (E) for PMN-PT single crystals was also calculated using the relations:

$$g_{33} = d_{33} / \varepsilon_o \varepsilon_r$$

$$E = e_{33}^2 / \varepsilon_o \varepsilon_r$$

where,

$$e_{33} = 1/g_{33}$$

3.1.1 Finite Element Analysis (FEA)

For more accurate results, the piezoelectric system equations of motion has been solved by the FEA using COMSOL Multiphysics software, the equations of motion can be written as (Xiong & Oyadiji., 2015):

$$[M]\ddot{u} + [C]\dot{u} + [K]u + [\chi]\varphi = P$$
$$Q + [\chi]u - [D]\varphi = 0$$

where [*C*] is the damping matrix, [*X*] is the piezoelectric coupling matrix, [*D*] is the dielectric stiffness matrix, u is the vector of nodal electric potential, P is the mechanical force vector and *Q* is the electrical charge vector. By operating the steady-state analysis, the FEA software can determine the nodal displacements, potentials gradients, and electrical flux densities.

4. Results and Discussion

4.1 Dielectric Measurements

Figure 2 shows the dielectric constants ε', and the dielectric loss constant ε" of PMN-PT single crystal measured at frequencies of 100 Hz, 1 kHz, 10 kHz, and 100 kHz, respectively. The temperature range was between room temperature and 130 °C. As expected in ferroelectrics, these parameters increase with increasing in temperature up to transition point, then quickly start decreasing as the temperature further increases. The maximum value of the dielectric constant are 9740, 9220, 8951, and, 8863 at 100 Hz, 1 kHz, 10 kHz, and 100 kHz, respectively. The maximum value of the dielectric loss are 311, 283, 229, and, 198 at 100 Hz, 1 kHz, 10 kHz, and 100 kHz, respectively, which PMN-PT single crystal between tetragonal ferroelectric and cubic paraelectric phases (Kochary et al., 2008). Figure 3 shows the temperature dependence of the ac conductivity measured at different frequency values. The fitting results of natural logarithm of ac conductivity versus inverse of the temperature in Kelvin scale for the PMN-PT single crystal give the activation energy (E_{ac}) values of 0.079, 0.082, 0.062, and 0.097 eV at 100 Hz, 1 kHz, 10 kHz, and 100 kHz, respectively.

The value of piezoelectric voltage constant (g_{33}) was calculated to be 18.2×10^{-3} m^2/C, then the Young's modulus value was calculated to be 72 GPa.

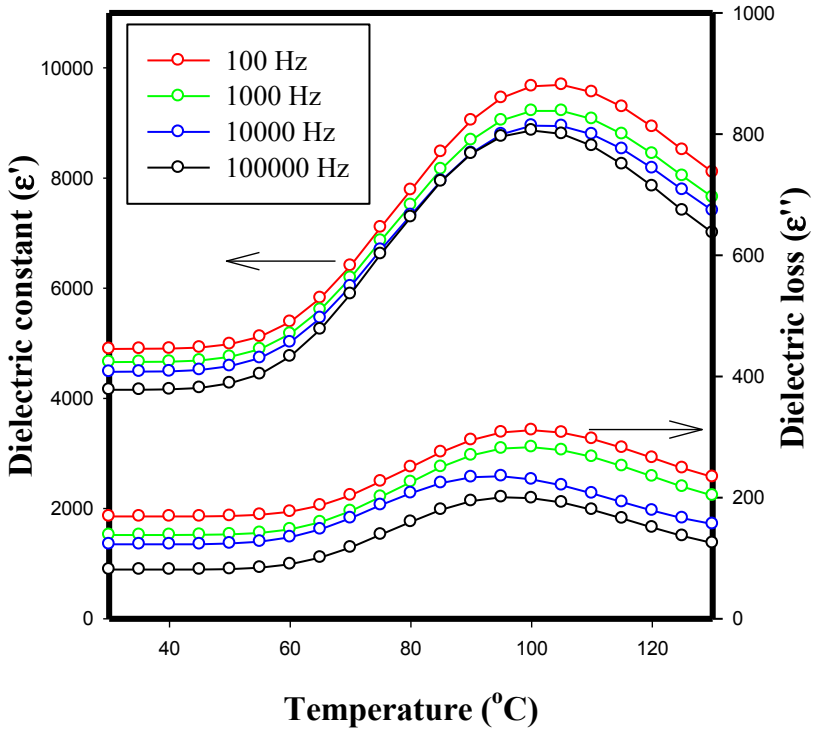

Figure 2. Temperature dependence of the dielectric constant and dielectric loss for a poled PMN-PT single crystal

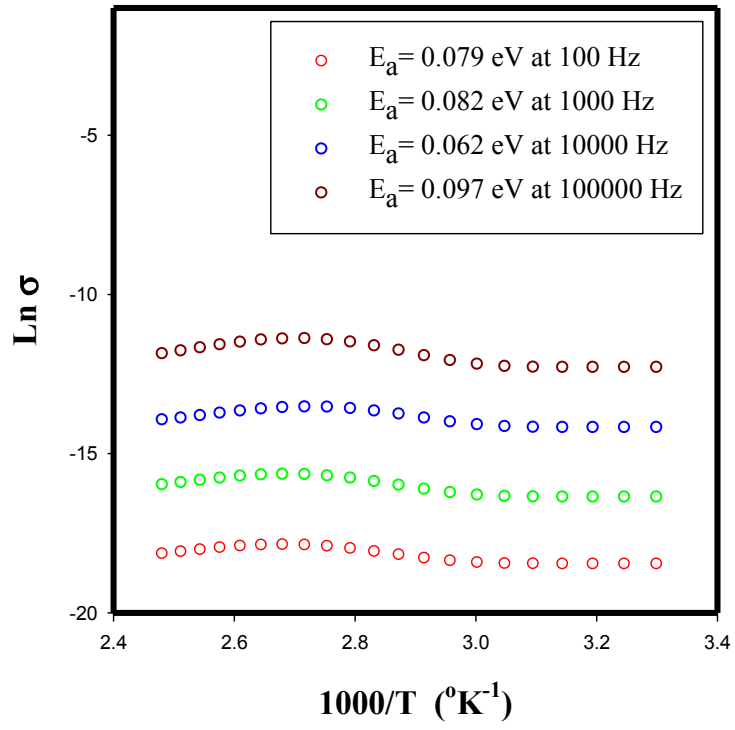

Figure 3. A plot of ac conductivity versus inverse of the temperature in Kelvin scale for the PMN-PT single crystal

4.2 Piezoelectric Energy Harvesting

In this section, we present the modeling and experimental results of the proposed PMN-PT VEH based on a lumped single-degree-of-freedom (SDOF). It is necessary here to calculate the mechanical damping ratio and the effective electromechanical coupling coefficient in order to find output voltage and power accurately. The mechanical damping ratio can be calculated from a comparison of the voltage amplitudes versus time (Priya. 2005). It has been found from Figure 4 that the calculated mechanical damping ratio is about 0.034. From difference natural frequency between an open- and a short-circuit piezoelectric material, the effective electromechanical coupling constant for a piezoelectric material bonded to a structure can be obtained (Park., 2003). The natural frequencies of an open- and a short- circuit piezoelectric material are about 56 and 51 Hz, respectively. The effective electromechanical coupling constant in the transverse mode was calculated to be 0.21.

The greatest electrical output amplitude of system can be obtained when the ambient frequency matches the natural frequency of VEH device. The base of VEH device was excited under a resonant frequency with acceleration of 1 g (9.81 m/s^2). The measured acceleration waveform in the accelerometer sensor and the output AC voltage of the device for this acceleration were displayed on a picoscope, as shown in Figure 5. It is convenient here to mention that the applied waveform was a sine wave and the sensitivity of the accelerometer sensor was 100 mV/g, the acceleration waveform was also a sine wave, and the output AC voltage value for the acceleration amplitude of the device was 800 mV. During the experiment, the applied acceleration on the device was maintained at 1 g by controlling the amplitude of the applied waveform.

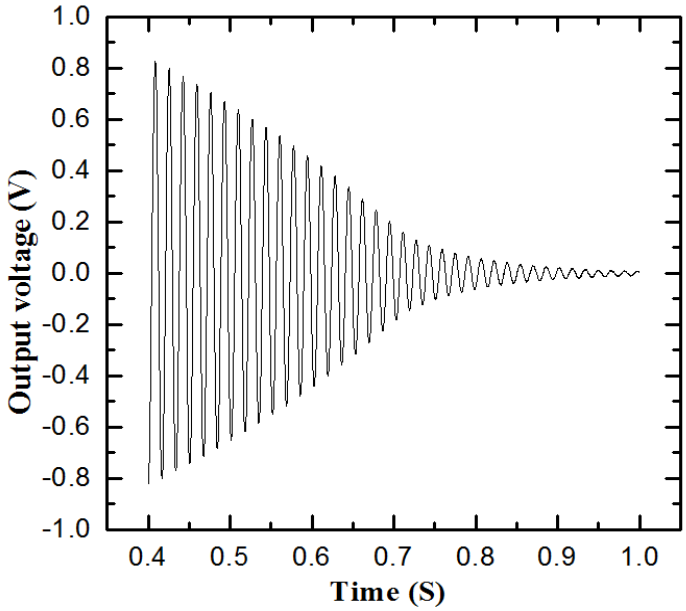

Figure 4. Measured output voltage versus time at first resonance frequency

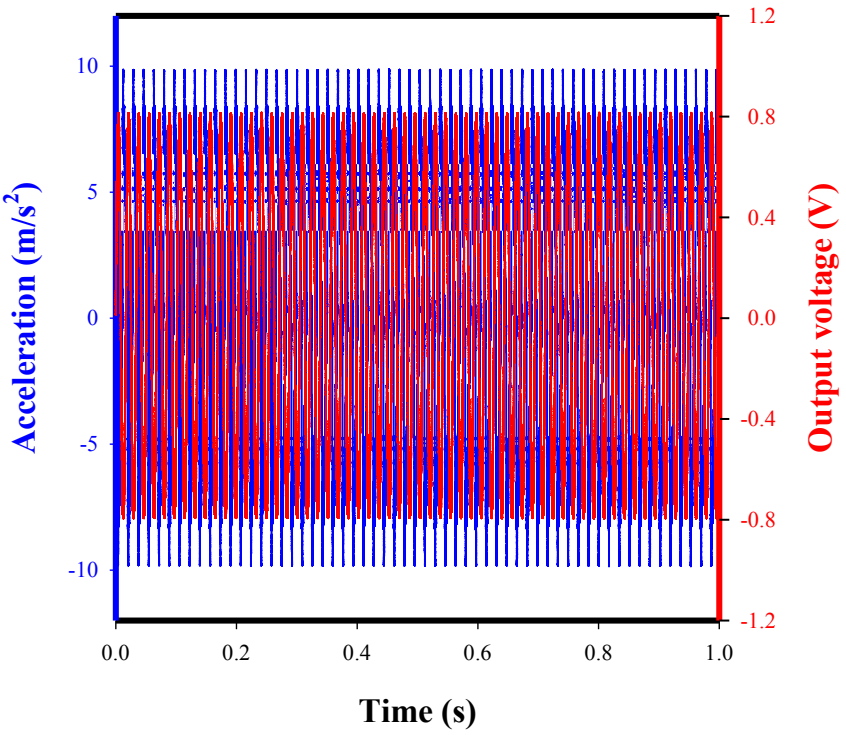

Figure 5. Measured output voltage and base acceleration at first resonance frequency

The frequency response functions (FRFs) in following graphs are normalized with respect to the gravitational acceleration for a convenient representation (i.e. the voltage and power FRF are divided by the gravitational acceleration, and gravitational acceleration square, respectively). Figure 6 shows the voltage output FRF around first resonance frequency at different load resistance values and measured displacement using laser at first resonance frequency. It can be seen from Figure 6 (a) that the voltage output increases monotonically with increasing load resistance and shows the maximum value at resonance frequency. Additionally, with increasing load resistance, the resonance frequency of each load resistance moves from the short circuit resonance frequency to the open circuit resonance frequency. As an example, in Figure 6 the maximum output voltage is obtained at short circuit resonance frequency of 51 Hz when load resistance is 100 Ω. However, when load resistance of 10 MΩ is used, the resonance frequency of the VEH becomes 56 Hz. It should be noted from Figure 6(b) that the tip displacement matches the maximum voltage FRF around the resonance frequency.

Figure 7 shows the average power FRF for PMN-PT VEH at a range of load resistances, R_L, from 100 Ω to 10 MΩ. It can be shown from Figure 7 that the maximum power of VEH is obtained for an optimum resistive load around 10 kΩ. Also, it can be seen from Figure 7 that the maximum power output of load resistance R_L=100 Ω at frequency 51 Hz, which is close to the short circuit resonance frequency is 5.24 μW and the maximum power output of R_L=10 MΩ at frequency 56 Hz, which is close to the open circuit resonance frequency is 37.15 μW. However, the maximum power output of R_L=10 kΩ, which is close to the optimum resistance value at frequency 52 Hz was 141.25 μW

For resonance frequency at 51 Hz, variation in the output voltage and average electrical power with load resistance is given by Figure 8. The overhang volume and the mass of the cantilever are about 0.300 cm^3 and 6.03 g, respectively. The maximum power density (power per volume) and the specific power (power per mass) of the device are then 5.2 μW/ (g^2 cm^3) and 0.262 mW/ (g^2 kg), respectively at optimum resistance of 7 kΩ. It can be seen from Figure 8 that the experimental and theoretical results are in good agreement. The voltage increases with load resistance (R_L) since the VEH acts as a capacitor during vibration and discharges to a lesser extent as the load resistance, and the associated RC time constant, increases. The optimum power is at the condition $2\pi.f.\ R_L.C=1$ where C is capacitance of the PMN-PT single crystal element (Chang & Hsu., 2013); for example at 51 Hz the optimum load resistance is 58.8 kΩ based on a device capacitance of 53.1 nF which is why the power level with load resistance flattens out in at 7 kΩ in Figure 8.

In last step, the AC output voltage has been converted into DC output voltage then stored in a rechargeable battery using an AC-DC circuit that shown in Figure 1(a). The rechargeable battery used in this study is CMOS Battery Lithium and have a nominal operating voltage of 3.0 V. The process has been executed using the excitation frequency of 51 Hz and optimum resistance of 7 kΩ under base excitation of 1 g. Figure 9 shows the results of the output voltage versus time that registered from picoscope during charging the battery. As can be seen from Figure 9 that the output voltage is increased to constant value of 2.88 V which is approximately 92% of full charge of rechargeable battery.

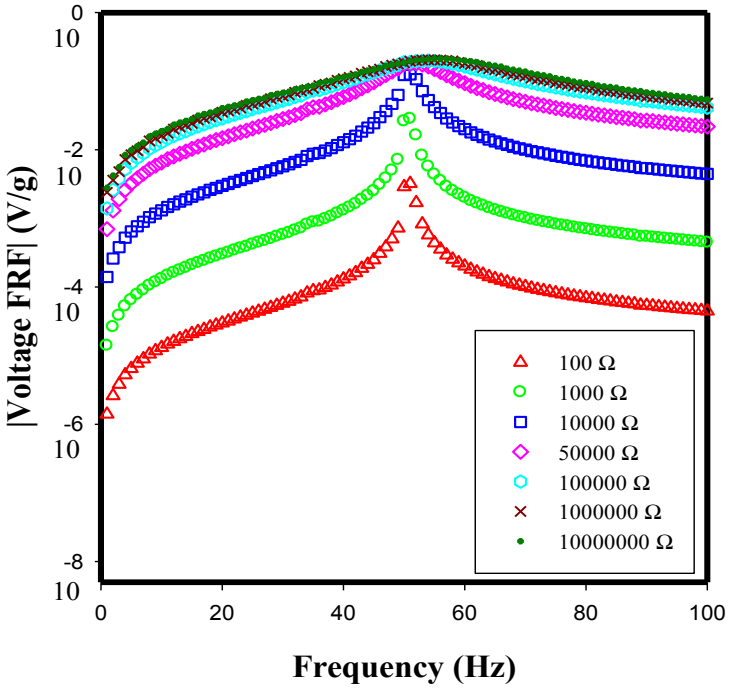

(a)

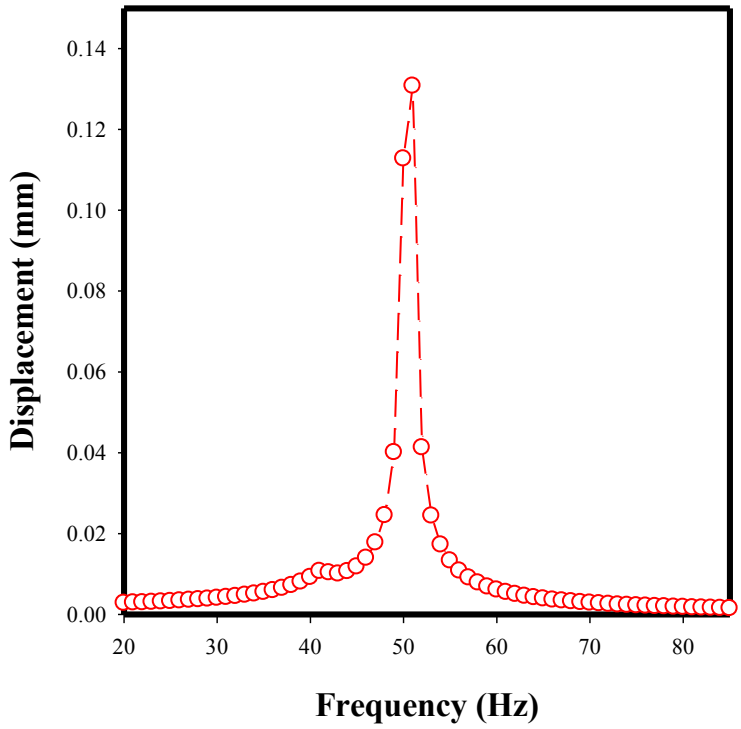

(b)

Figure 6. (a) Voltage FRF for seven different values of load resistance around first resonance frequency (b) displacement measured versus frequency using laser at first resonance frequency of load resistance R_L=10 kΩ.

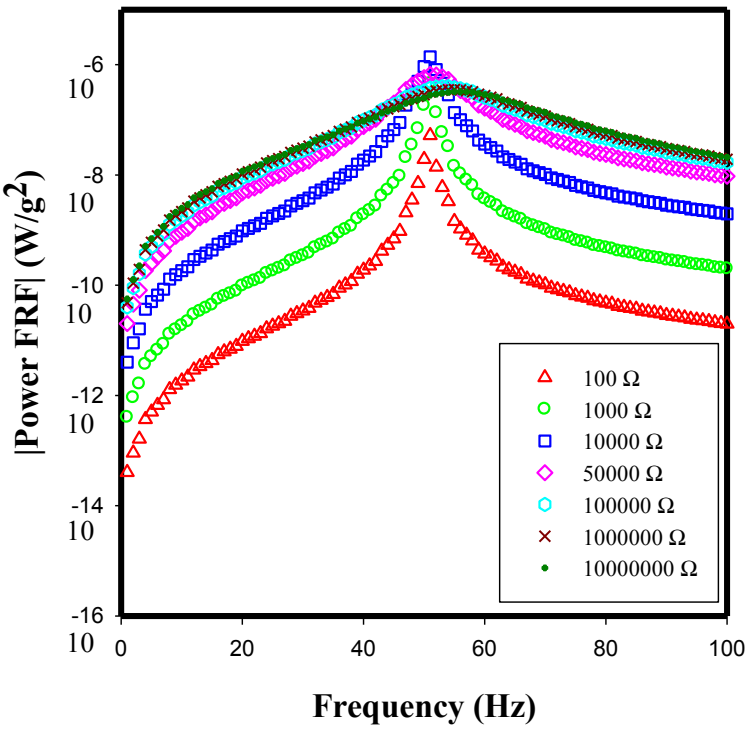

Figure 7. Power FRF for seven different values of load resistance around first resonance frequency

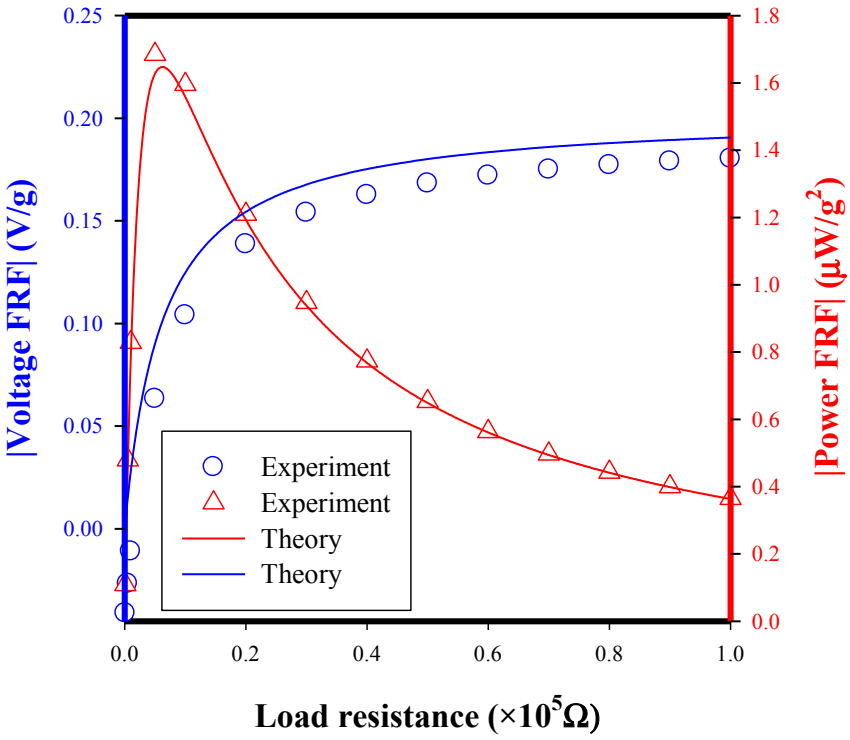

Figure 8. Voltage and power FRF versus load resistance at first resonance frequency

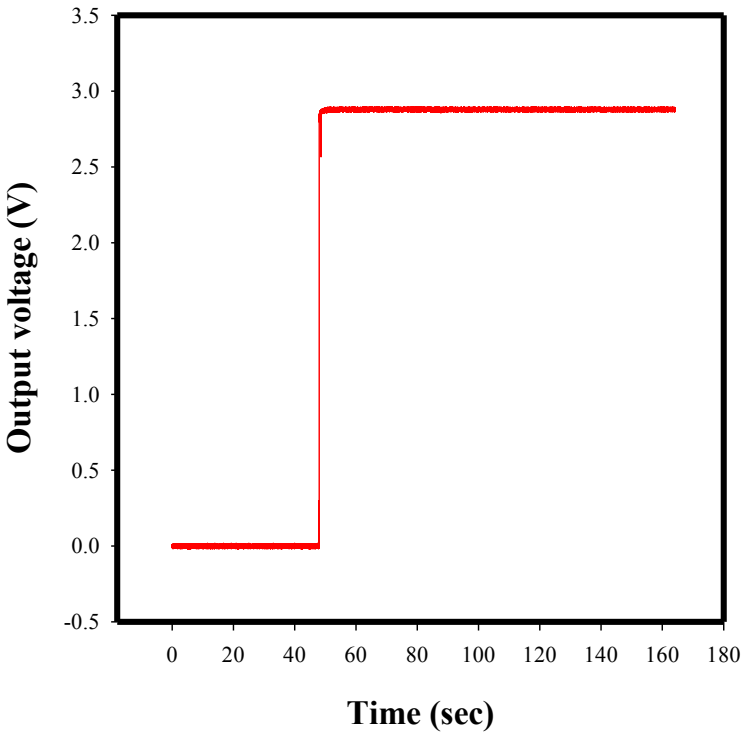

Figure 9. Output voltage stored in rechargeable battery versus time

4.3 The verification by the experiment and FEA using COMSOL

The output peak voltage and power of the PMN-PT VEH are also simulated by numerical method using the commercial finite element analysis package (COMSOL). The VEH consists of a PMN-PT piezoelectric thick film positioned at clamped-end with a proof mass mounted on the other end. The PMN-PT piezoelectric thick film has a ground electrode embedded within it and other electrode on the exterior surfaces of the cantilever beam. Figure 10 (a and b) shows the finite element mesh and first mode shape of PMN-PT VEH, respectively. As can be seen from Figure 10(a) that the voltage of top surface of PMN-PT film is coupled and a load resistor is connected between the top surface of piezoelectric layer and the top surfac of aluminum beam. The voltage of top surface of piezoelectric layer, which is output voltage across load resistor, is solved when the cantilever beam is loaded with an inertial acceleration 10 m/s^2 under solution of frequency domain technique.

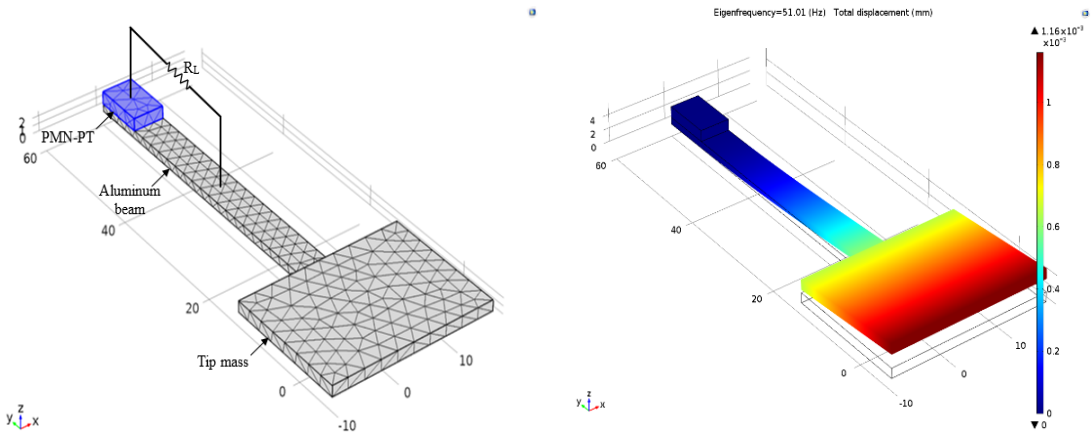

(a) (b)

Figure 10. (a) The finite element mesh and (b) the first mode shape of piezoelectric cantilever.

The frequency dependence of output peak voltage and power for the experimental optimum load resistances R_L = 7 kΩ is simulated to compare with that of the shear mode piezoelectric cantilever with PMN-PT single crystal. The model predictions of COMSOL numerical solutions and experimental measurements are given in Figures 11 and 12, respectively. The output peak voltage versus frequency curves simulated by proposed model are very close to the experimental and numerical results, indicating that the proposed model is effective to predict the frequency dependence of output peak voltage for the shear mode piezoelectric cantilever.

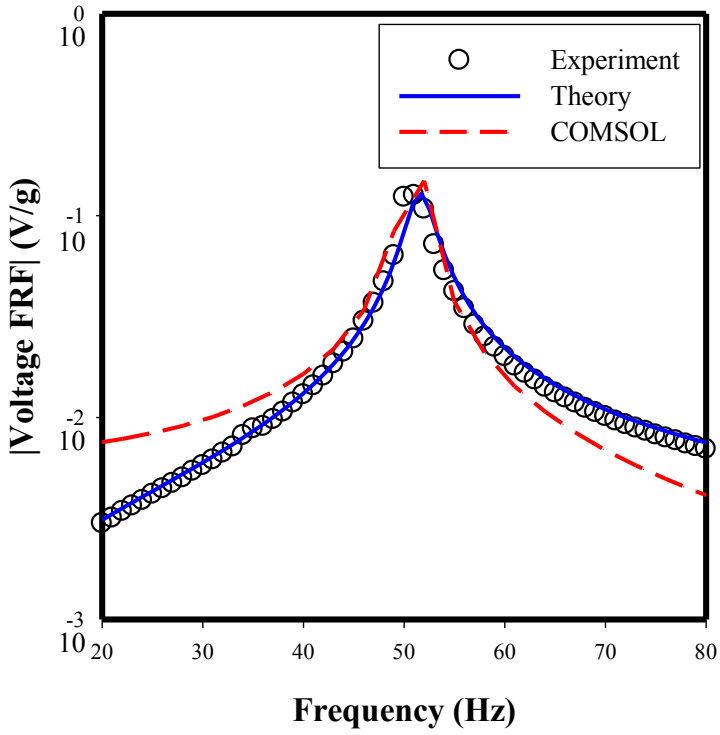

Figure 11. The model predictions, experimental measurements and numerical results of output voltage FRF at optimum resistance R_L=7 kΩ.

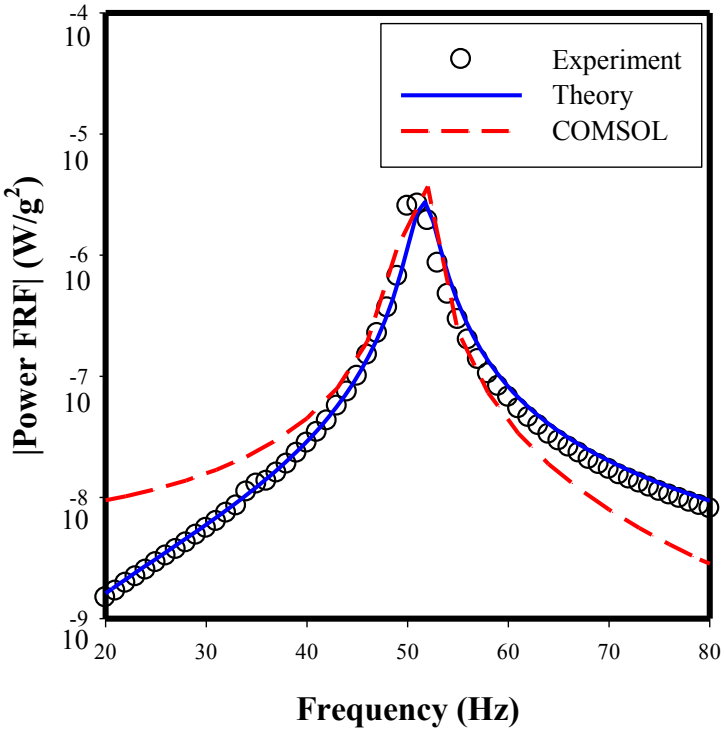

Figure 12. The model predictions, experimental measurements and numerical results of output power FRF at optimum resistance R_L=7 kΩ.

4.4 Piezoelectric and Pyroelectric Energy Harvesting

Figure 13 shows the variation of pyroelectric coefficient with temperature where this parameter increases as temperature increases, which is typical of ferroelectrics. Pyroelectric voltage output of VEH response has been tested versus temperature under different frequency values. In this case the VEH showed increasing in output voltage with temperature, the AC output voltage was increased from 0.35 V to 0.65 V, from 0.27 V to 0.78 V, and from 0.34 V to 0.45 V at frequency values of 8 Hz, 11 Hz, and 30 Hz, respectively.

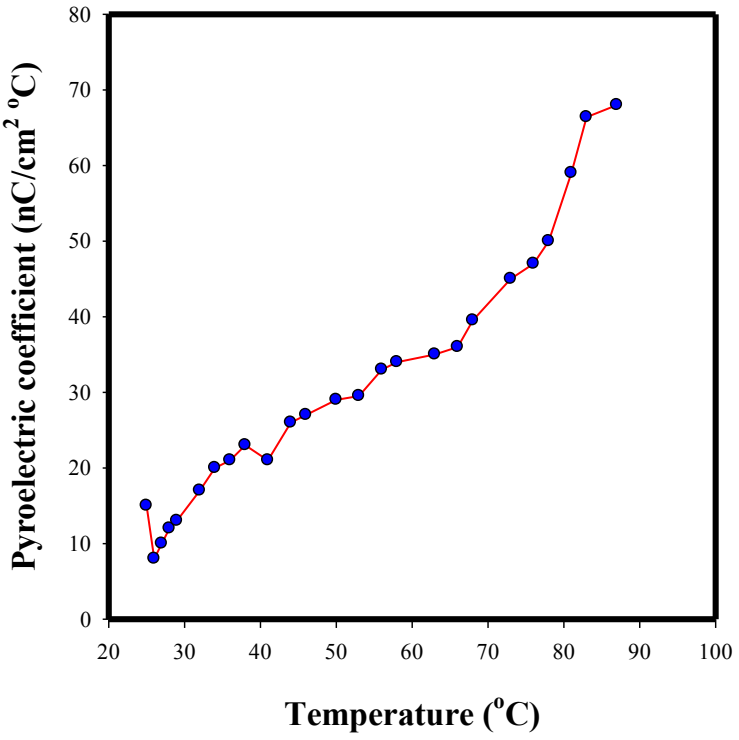

Figure 13. Variation of the pyroelectric coefficient with temperature for PMN-PT single crystal

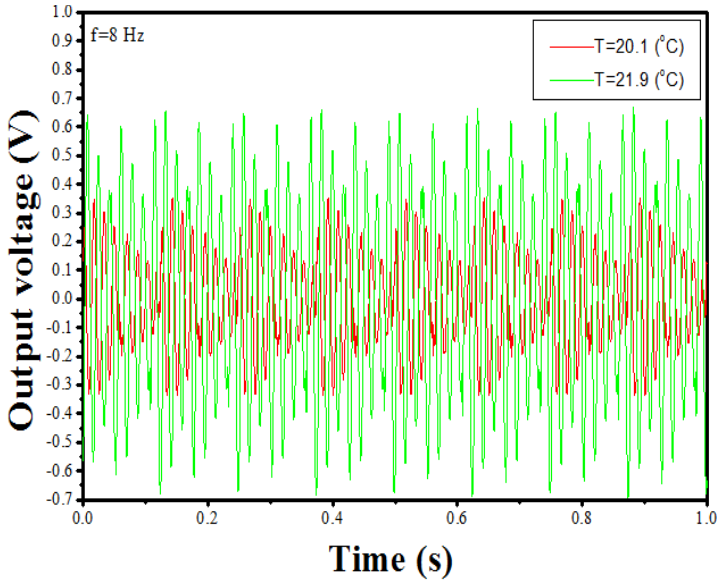
f=8 Hz
T=20.1 (°C)
T=21.9 (°C)
Output voltage (V)
Time (s)

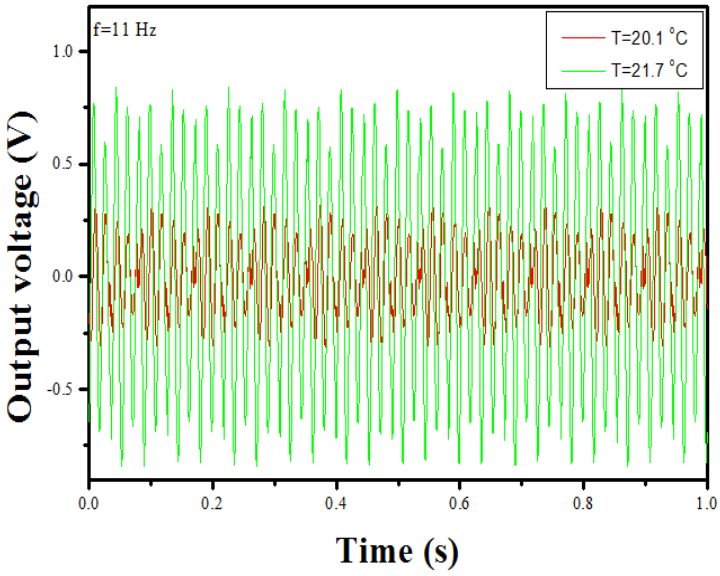
f=11 Hz
T=20.1 °C
T=21.7 °C
Output voltage (V)
Time (s)

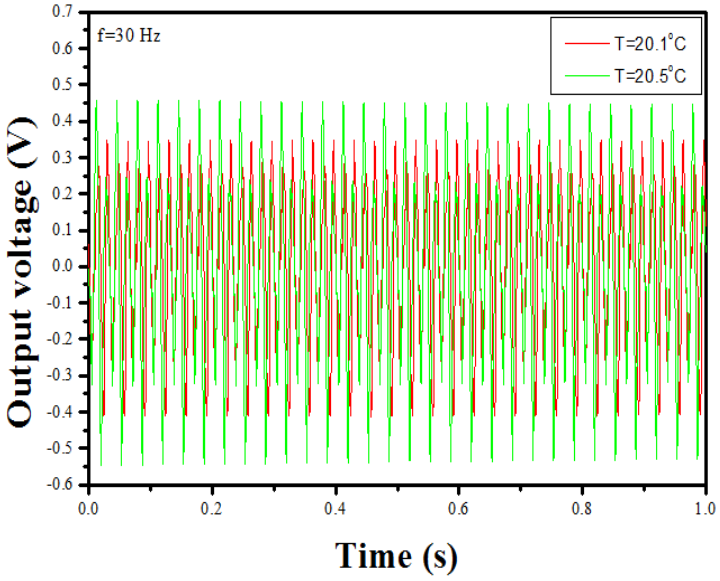

Figure 14. Variation of the output voltage versus temperature for PMN-PT single crystal at frequency of (a) 8 Hz, (b) 11 Hz, and (c) 30 Hz.

5. Conclusions

This article presents the study of multisource piezo/pyro effect on a PMN-PT with (67:33) composition single crystal grown in our laboratory via a vertical gradient freeze method with no flux. Piezoelectric energy harvesting of PMN-PT single crystal has been tested using a unimorph mechanical cantilever design with tip mass. A theoretical SDOF model is utilized for predicting the dynamic response of the proposed Vibration Energy Harvester (VEH). The maximum power density at resonance frequency 51 Hz and optimum resistance of 7 kΩ was 5.2 μW/ (g^2 cm^3) under acceleration of vibration base of 1 g. The measured values of electrical output parameters showed a good agreement with theoretical and modelling results using MATLAB and COMSOL Multiphysics respectively. The present study has also showed the capability of PMN-PT piezoelectric device to recharge a rechargeable battery at resonance frequency, optimum resistance and under base excitation of 1 g. Finally, Performance of a multisource energy harvester to simultaneously harvesting thermal and mechanical energies utilizing a single crystal PMN-PT patch is investigated in this study. In this case, it is demonstrated that increasing in output voltage with temperature gradient; the AC output voltage was increased from 0.35 V to 0.65 V, from 0.27 V to 0.78 V, and from 0.34 V to 0.45 V at frequency values of 8 Hz, 11 Hz, and 30 Hz, respectively.

Acknowledgements

The authors gratefully acknowledge support for this work through the National Science Foundation grant #EPSCoR R-II-3 (EPS-1158862). Authors thank Dr. Chance M. Glenn, Dean, College of Engineering, Technology, and Physical Sciences.

References

Park, S. E., & Shrout, T. R. (1997). Characteristics of relaxor-based piezoelectric single crystals for ultrasonic transducers. Ultrasonics, Ferroelectrics, and Frequency Control, IEEE Transactions on, 44(5), 1140-1147.

Bowen, C. R., Taylor, J., LeBoulbar, E., Zabek, D., Chauhan, A., & Vaish, R. (2014). Pyroelectric materials and devices for energy harvesting applications. Energy & Environmental Science, 7(12), 3836-3856.

Roundy, S., & Wright, P. K. (2004). A piezoelectric vibration based generator for wireless electronics. Smart Materials and structures, 13(5), 1131.

Radziemski, L. J., & Lynn, K. G. (2004). U.S. Patent No. 6,737,789. Washington, DC: U.S. Patent and Trademark Office.

Green, C., Mossi, K. M., & Bryant, R. G. (2005, January). Scavenging energy from piezoelectric materials for wireless sensor applications. In ASME 2005 International Mechanical Engineering Congress and Exposition (pp. 93-99). American Society of Mechanical Engineers

Ren, K., Liu, Y., Geng, X., Hofmann, H. F., & Zhang, Q. M. (2006). Single crystal PMN-PT/epoxy 1-3 composite for energy-harvesting application. ieee transactions on ultrasonics, ferroelectrics, and frequency control, 53(3), 631-638.

Badel, A., Benayad, A., Lefeuvre, E., Lebrun, L., Richard, C., & Guyomar, D. (2006). Single crystals and nonlinear process for outstanding vibration-powered electrical generators. IEEE transactions on ultrasonics, ferroelectrics, and frequency control, 53(4), 673-684.

Song, H. J., Choi, Y. T., Wang, G., & Wereley, N. M. (2009). Energy harvesting utilizing single crystal PMN-PT material and application to a self-powered accelerometer. Journal of Mechanical Design, 131(9), 091008.

Kim, K. B., Hsu, D. K., Ahn, B., Kim, Y. G., & Barnard, D. J. (2010). Fabrication and comparison of PMN-PT single crystal, PZT and PZT-based 1-3 composite ultrasonic transducers for NDE applications. Ultrasonics, 50(8), 790-797.

Leadbetter, J., Brown, J. A., & Adamson, R. B. (2013, June). The design of ultrasonic lead magnesium niobate-lead titanate (PMN-PT) composite transducers for power and signal delivery to implanted hearing aids. In Proceedings of Meetings on Acoustics (Vol. 19, No. 1, p. 030029). Acoustical Society of America

Hwang, G. T., Park, H., Lee, J. H., Oh, S., Park, K. I., Byun, M., ... & Kwon, H. (2014). Self-Powered Cardiac Pacemaker Enabled by Flexible Single Crystalline PMN-PT Piezoelectric Energy Harvester. Advanced materials, 26(28), 4880-4887.

Kazys, R. J., Sliteris, R., & Sestoke, J. (2015). Application of PMN-32PT piezoelectric crystals for novel air-coupled ultrasonic transducers. Physics Procedia, 70, 896-900.

Hong, Y. K., Park, H. K., Lee, S. Q., Moon, K. S., & Levy, M. (2004, September). Fabrication of a piezoelectric biosensor based on a PZN-PT/PMN-PT single crystal thin film. In Optics East (pp. 140-147). International Society for Optics and Photonics.

Uchino, K. (2009). *Ferroelectric Devices 2nd Edition*. CRC press. (p228, CH8)

Bai, Y., Cheng, Z. Y., Bharti, V., Xu, H. S., & Zhang, Q. M. (2000). High-dielectric-constant ceramic-powder polymer composites. *Applied Physics Letters*, *76*(25), 3804-3806.

Choi, S. W., Shrout, R. T., Jang, S. J., & Bhalla, A. S. (1989). Dielectric and pyroelectric properties in the Pb (Mg1/3Nb2/3) O3-PbTiO3 system.*Ferroelectrics*, *100*(1), 29-38.

Zawilski, K. T., Custodio, M. C. C., DeMattei, R. C., Lee, S. G., Monteiro, R. G., Odagawa, H., & Feigelson, R. S. (2003). Segregation during the vertical Bridgman growth of lead magnesium niobate–lead titanate single crystals. Journal of crystal growth, 258(3), 353-367.

Tang, G., Yang, B., Liu, J. Q., Xu, B., Zhu, H. Y., & Yang, C. S. (2014). Development of high performance piezoelectric d 33 mode MEMS vibration energy harvester based on PMN-PT single crystal thick film. Sensors and Actuators A: Physical, 205, 150-155.

Seung, E. M., Sang, K. L., Hyung-Kun, L., Jae-Woo, L., Yil-Suk, Y., & Jongdae, K. (2011). Analysis of Vibration-energy-harvesting Devices based on a Piezoelectric Single Crystal Beam. Journal of Korean Physical Society, 58, 645.

Ren, B., Or, S. W., Zhang, Y., Zhang, Q., Li, X., Jiao, J., ... & Luo, H. (2010). Piezoelectric energy harvesting using shear mode 0.71 Pb (Mg1/3Nb2/3) O3–0.29 PbTiO3 single crystal cantilever. Applied Physics Letters, 96(8), 083502.

Zhou, L., Sun, J., Zheng, X. J., Deng, S. F., Zhao, J. H., Peng, S. T., ... & Cheng, H. B. (2012). A model for the energy harvesting performance of shear mode piezoelectric cantilever. *Sensors and Actuators A: Physical*, *179*, 185-192.

Song, H. J., Choi, Y. T., Wang, G., & Wereley, N. M. (2009). Energy harvesting utilizing single crystal PMN-PT material and application to a self-powered accelerometer. *Journal of Mechanical Design*, *131*(9), 091008.

Moon, S. E., Lee, S. Q., Lee, S. K., Lee, Y. G., Yang, Y. S., Park, K. H., & Kim, J. (2009). Sustainable vibration energy harvesting based on Zr-doped PMN-PT piezoelectric single crystal cantilevers. ETRI journal, 31(6), 688-694.

Uršič, H., & Kosec, M. (2011). *Relaxor-ferroelectric PMN-PT Thick Films*. INTECH Open Access Publisher.

Kochary, F., Aggarwal, M. D., Batra, A. K., Hawrami, R., Lianos, D., & Burger, A. (2008). Growth and electrical characterization of the lead magnesium niobate-lead titanate (PMN-PT) single crystals for piezoelectric devices. Journal of Materials Science: Materials in Electronics, 19(11), 1058-1063.

Chang, W. Y., & Hsu, C. H. (2013). Electromechanical characteristics of Polyvinylidene Fluoride for flexible electronics. Transactions of the Canadian Society for Mechanical Engineering, 37(3).

Priya, S. (2005). Modeling of electric energy harvesting using piezoelectric windmill. Applied Physics Letters, 87(18), 184101.

Park, C. H. (2003). Dynamics modelling of beams with shunted piezoelectric elements. *Journal of Sound and Vibration*, *268*(1), 115-129.

Erturk, A., Bilgen, O., & Inman, D. J. (2008). Power generation and shunt damping performance of a single crystal lead magnesium niobate-lead zirconate titanate unimorph: Analysis and experiment. Applied Physics Letters, 93(22), 224102.